Doubly excited electron-ion angular momentum transfer in parity-unfavored multiphoton ionization

Meng Han [ORCID],[1] Peipei Ge,[1] Yiqi Fang,[1] Xiaoyang Yu,[1] Zhengning Guo,[1] Yongkai Deng,[1] Chengyin Wu [ORCID],[1] Qihuang Gong,[1,2,4] and Yunquan Liu[1,2,3,4,*]

[1]*State Key Laboratory for Mesoscopic Physics, School of Physics, Frontiers Science Center for Nano-optoelectronics and Collaborative Innovation Center of Quantum Matter, Peking University, Beijing 100871, China*
[2]*Collaborative Innovation Center of Extreme Optics, Shanxi University, Taiyuan, Shanxi 030006, China*
[3]*Center for Applied Physics and Technology, HEDPS, Peking University, Beijing 100871, China*
[4]*Beijing Academy of Quantum Information Sciences, Beijing 100193, China*

We observe the parity-unfavored photoelectron emission in multiphoton single ionization of krypton atoms in an intense ultraviolet laser field. With systematic experiments of successively varying the light ellipticity and intensity, we identify that this parity-unfavored emission is associated with the first excited ionic state via a resonant pathway. We reveal an abnormal Coulomb asymmetry of the parity-unfavored photoelectron emission in elliptically polarized fields when the ellipticity is less than 0.3. The simulation using the time-dependent Schrödinger equation based on single-active-electron approximation fails to reproduce the experiment. We attribute the experimental observations to the angular momentum correlation between the resonantly excited electron and the spin-orbit excited ion. Our results demonstrate that the well-known picture of the angular momentum transfer in multiphoton ionization is broken and instead that the electron shares the spin angular momenta of photons with the ion as an effect of electron correlations.

Photoionization of atoms and molecules is a fundamental many-body dynamical process, governed by energy and momentum conservations. The conservation laws dictate that the absorbed photons transfer their energy and momentum to the electron and its parent ion. The electron-nuclear sharing of these physical quantities and its underlying mechanism hence become an important topic in strong-field ionization [1–7]. For example, the photon energy deposition has been extensively studied in multiphoton ionization dissociation of molecules [1–4], and the photon linear momentum deposition in tunneling ionization has been debated for the last decade [5,6] and was recently resolved by a well-designed experiment [7]. By contrast to the depositions of the photon energy and linear momentum, the electron-nuclear sharing of the photon spin angular momentum, which is associated with the light polarization, received less attention. It is usually assumed that the spin angular momentum is totally transferred to the electron forming its orbital angular momentum, manifesting as the selection rule of the electron magnetic quantum number m. In a linearly polarized field, the selection rule dictates that the electron emits dominantly along the light polarization, i.e., m is confined to zero [8]. Therefore, it would be interesting that photoelectrons emit dominantly and vertically with respect to the light polarization, and any violation of this angular momentum transfer rule will provide direct insight into the many-body dynamics.

The crosswise electron emission was studied in single-photon ionization regime by Fano and Dill [9–12], dubbed as the parity-unfavored transition [11]. It has been revealed as a typical feature for the ionization of open-shell atoms owing to therein anisotropic electron-ion interaction [13,14]. However, for the closed-shell atoms (such as krypton as we study here) the atomic potential felt by the outmost electron is isotropic. Thus the single-active-electron approximation and the consequently established selection rule seem robust. Actually, when removing an electron from a closed-shell atom, the spin-orbit coupling of valence electrons (or the equivalent electron hole) in the residual ion will come into play. For example, the remaining five p electrons in the krypton ion ($4p^5$) will perform the L-S coupling, splitting the ion into two ionic states, $^2P_{3/2}$ (the ground state with the angular momentum $J_i = 3/2$) and $^2P_{1/2}$ (the first excited state with $J_i = 1/2$). Recently, this spin-orbit effect has attracted much attention in the strong-field community, such as producing spin-polarized photoelectrons using circularly polarized fields [15–19], real-time imaging the electron hole in the ion [20–23], and measuring the relative ionization time delay between the two ionic states [24]. However, the residual ion is always treated as the spectator during the angular momentum transfer process in photoionization and its angular momentum correlation with the photoelectron has not been revealed.

In this Rapid Communication, we present an experimental and theoretical study of multiphoton single ionization of krypton atoms in an ultraviolet laser field at the wavelength of 400 nm. When the light is linearly polarized, we observe the parity-unfavored photoelectron emission pertained to the excited ionic state $^2P_{1/2}$, whose electron yield is anomalously larger than that from the ground ionic state $^2P_{3/2}$. Moreover, when the ellipticity is less than 0.3 we reveal that the parity-unfavored photoelectron structure shows an abnormal rotation. The simulation based on single-electron dynamics
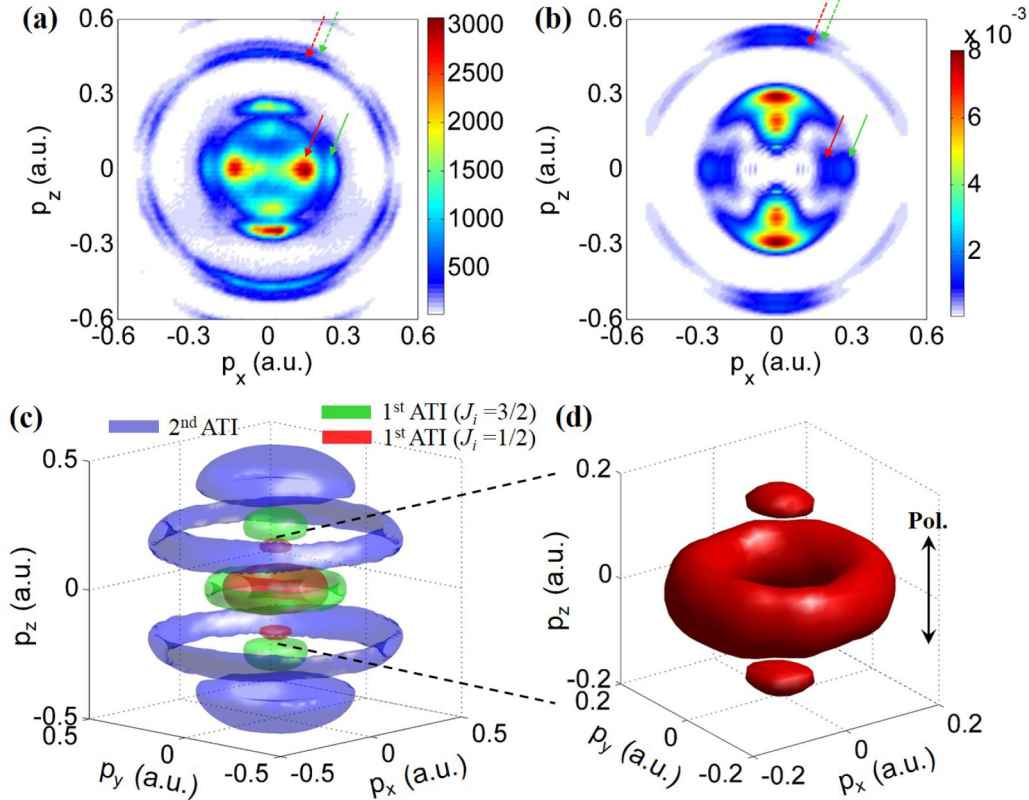
*yunquan.liu@pku.edu.cn

FIG. 1. Photoelectron momentum distributions of krypton atoms ionized by a linearly polarized 400-nm light field along the z axis. (a) Two-dimensional momentum slice of the measurement with integrating p_y from -0.15 to 0.15 a.u. (b) TDSE simulation within single-active-electron approximation. In (a) and (b), the ATIs corresponding to the excited (ground) ionic state are marked with the red (green) arrows, and the first- (second-) order ATIs are marked with the solid (dashed) arrows. (c) Measured three-dimensional photoelectron momentum distribution. The isocount surface of the second order ATI is not divided into the two ionic states due to the low counts and their close momentum spacing. (d) The enlarged low-energy part of (c) to strength the anomalous vertically emitted photoelectron structure of the first-order ATI from the excited ionic state. The double-sided arrow indicates the polarization direction of the light field.

fails to reproduce these observations. With the help of experiments of successively varying the light intensity, we identify that the parity-unfavored photoelectron emission originates from the angular momentum transfer between the resonantly excited Rydberg electron and the spin-orbit excited ion. In circularly polarized fields, the electronic resonance pathway is prohibited and thus these abnormal phenomena disappear as we confirmed experimentally.

Experimentally, the fundamental laser pulses (800 nm, 25 fs, p polarization) were delivered from a multipass Ti:sapphire laser amplifier operating at 3 kHz. We obtained the second harmonic (400 nm, 35 fs, s polarization) via frequency doubling using a 200-μm-thick β-barium borate (BBO) crystal, and the remaining fundamental field was removed using a dichroic mirror. For the experiments of continuously varying the light ellipticity or intensity, we guided the light beam through a thin-film polarizer, $\lambda/2$ and $\lambda/4$ wave plates. The $\lambda/2$ wave plate was mounted in a motorized rotary stage and we successively rotated it in the x-z plane when acquiring data. The laser pulses propagated along the y axis and were focused into a skimmed supersonic jet of krypton gas at the maximum intensity of $\sim 8.0 \times 10^{13}$ W/cm^2, which was calibrated by the slope of the above-threshold ionization (ATI) peaks with respect to the laser intensity [25].

We measured three dimensional momenta of photoelectrons using cold target recoil ion momentum spectroscopy (COLTRIMS) [26,27]. Only single ionization events were analyzed and presented. The static electric (~ 3.2 V/cm) and magnetic (~ 5.4 G) fields were applied along the z axis in the spectrometer to collect the charged fragments.

The measured photoelectron momentum distribution in a linearly polarized field at the intensity of $\sim 3.2 \times 10^{13}$ W/cm^2 is shown in Fig. 1(a). There are two sets of ATI structures, corresponding to the two ionic states. The one with a lower energy is contributed from the excited ionic state $^2P_{1/2}$. The first-order ATI from $^2P_{1/2}$ resembles a d_0 ($l = 2$, $m = 0$) wave, except for the unusual phenomenon that the yield along the perpendicular direction is much greater than that along the polarization direction [also see Figs. 1(c) and 1(d) for the three-dimensional distribution]. By contrast, the photoelectron structure from the ground ionic state peaks along the light polarization, approaching a standard d_0 wave for the first-order ATI. Moreover, the angle-integrated spectrum indicates that the total photoelectron yield from the excited ionic state is larger than that from the ground ionic state [see the blue curve in Fig. 2(g)], which is also not expected [15–19] since the excited ionic state has a higher ionization potential ($\Delta I_p = 0.67$ eV).
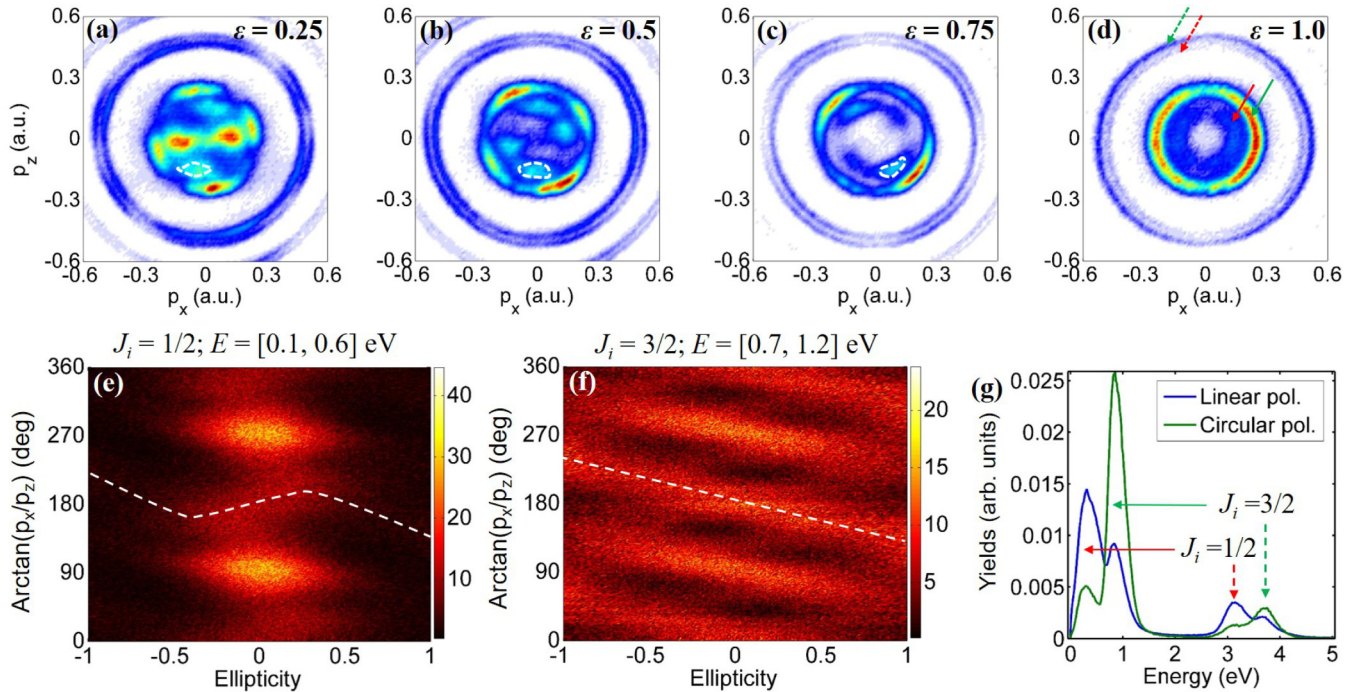
FIG. 2. (a)–(d) Two-dimensional photoelectron momentum distributions in the polarization plane at the ellipticity of 0.25, 0.5, 0.75, and 1.0, respectively. The momentum p_y is integrated from -0.15 to 0.15 a.u. The white dashed circles are used to mark the abnormal rotation of the down lobe on the first-order ATI from the excited ionic state. The count axis, as well as the color scale, are linear. (e),(f) Ellipticity-resolved photoelectron angular distributions of the first-order ATIs from the excited (e) and the ground (f) ionic states. The integrated energy ranges are labeled on the top of the panels. The white dashed curves depict the rotating trend of the down lobe marked in (a)–(c) with respect to the ellipticity. (g) Angle-integrated photoelectron energy spectra at the ellipticity of 0.0 and 1.0.

Then, we measured photoelectron momentum distributions in elliptically polarized fields at the intensity of $\sim 3.2 \times 10^{13}$ W/cm^2. In the experiment, the light ellipticity (ε) was successively tuned from -1 (left circular) to 1 (right circular), and in the process the major axis of ellipses was fixed along the z axis. In Figs. 2(a)–2(d), we illustrate the photoelectron momentum distributions at the ellipticities of 0.25, 0.5, 0.75, and 1.0, respectively. Generally, in elliptically polarized fields the photoelectron momentum distribution will be tilted by the Coulomb field, dubbed as "Coulomb asymmetry" [28–30]. However, when checking our measured distributions, one can clearly observe that the rotation direction of the first-order ATI from the excited ionic state at the small ellipticity ($\varepsilon = 0.25$) is reversed relative to that from the ground ionic state. By contrast, at the large ellipticity ($\varepsilon = 0.75$) the photoelectron rotation directions from the two ionic states become the same.

In Figs. 2(e)–2(f), we illustrate the ellipticity-resolved photoelectron angular distributions of the first-order ATIs from the two ionic states. In this representation, one can intuitively observe the rotation trace of each lobe on the ATI with respect to the ellipticity. Our results show that the photoelectron rotation direction corresponding to the excited ionic state is abnormal when $|\varepsilon| < 0.3$. More specifically, the up-down lobes rotate in the opposite helicity with respect to the left-right lobes. As to the case of the ground ionic state, all the lobes on the ATI rotate in the same helicity within the whole ellipticity range [see the white dashed curves in Figs. 2(e) and 2(f) for the rotation traces from the two ionic states].

To judge whether single-electron dynamics is the origin of above observations, we resort to the time-dependent Schrödinger equation (TDSE) [31,32] based on single-active-electron approximation, which is an *ab initio* method including most influence factors except the many-body effect. In the simulation, an effective model potential $V_{\text{eff}} = -[Z + (Z_{\text{full}} - Z)e^{-r_s \cdot r}]/r$ was used, where $Z = 1$ and $Z_{\text{full}} = 36$ are the asymptotic ion charges as $r \to \infty$ and $r \to 0$, respectively. The screening length $r_s = 7.7534$ is tuned to match $I_p = 0.539$ a.u. (14.67 eV) for the excited ionic state, and $r_s = 7.7631$ to match $I_p = 0.515$ a.u. (14.0 eV) for the ground ionic state. The ionization channels of the two ionic states are calculated independently. The used laser field is expressed as $\boldsymbol{E} = E\varepsilon/\sqrt{1+\varepsilon^2}\sin(\omega t)\hat{\boldsymbol{x}} + E/\sqrt{1+\varepsilon^2}\cos(\omega t)\hat{\boldsymbol{z}}$ with a 16-cycle $\sin^2$-shape envelope, where $E = 0.03$ a.u. is the electric-field amplitude and $\omega = 0.114$ a.u. is the laser frequency of 400 nm.

After summing the simulated results from the two ionic states incoherently, we illustrate the photoelectron momentum distribution at the linear polarization in Fig. 1(b). The distribution exhibits that the two first-order ATIs are both close to the standard d_0 wave; i.e., no parity-unfavored structure is observed. And the photoelectron yield from the excited ionic state is less than that from the ground ionic state as expected. We further illustrate the simulated photoelectron momentum distribution at the ellipticity of 0.25 in Fig. 3. Although the rotation angle of the up-down lobes is smaller than that of the left-right lobes, they still rotate in the same helicity. Overall,
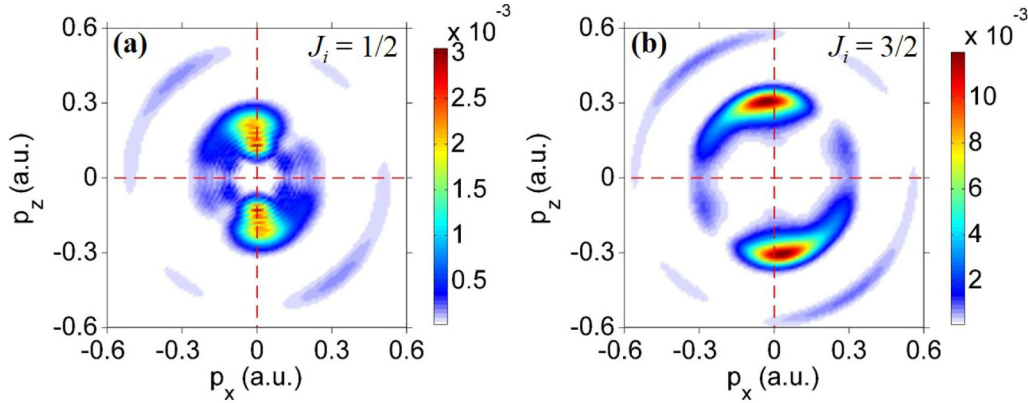
FIG. 3. (a),(b) TDSE simulations of the photoelectron momentum distributions at the ellipticity of 0.25 for the excited ($J_i = 1/2$) and the ground ($J_i = 3/2$) ionic states, respectively.

the difference between the two ionic states is not obvious, except for their energy separation.

After comparing the TDSE simulation with the measurement, one can rule out the mechanism of single-electron dynamics. The many-body dynamics might be important. We then performed the experiment at the linear polarization with successively varying the light intensity. In Fig. 4(a), we illustrate the measured intensity-resolved photoelectron energy spectrum. One clearly observes that the energy of the abnormal ATI from the excited ionic state does not change nearly (at ~0.55 eV) when varying the light intensity, indicating that there is a strong resonant Rydberg state participated. This is because the high Rydberg states and the ionization threshold possess the same Stark-shift energy in a light field [25].

In Fig. 4(c), we illustrate the relevant energy levels of krypton to understand the ionization dynamics in linear polarization. After checking the energy, we identify that the observed resonant state is the $5p$ state (11.5 eV), which is populated by absorbing four photons from the ground state ($4p^6$). From the resonant $5p$ state, the electron then absorbs one photon ($h\nu \sim 3.05$ eV) and its energy exceeds the ionization threshold of the atom (i.e., $I_p = 14.0$ eV for the ground ionic state). However, at this instant the atom is not broken up, since the ion can absorb the excessive energy through the spin-orbit coupling of the residue electrons. Thus, the outmost electron is still bound into a Rydberg state. Finally, when the excited ion relaxes to its ground state, the Rydberg electron obtains the energy released by the ion and then emits from the atom, which is also known as autoionization [33,34]. In previous studies on the autoionization [35–37], only the energy transfer between electron and ion is involved and their angular momentum correlation is yet unclear.

Here we demonstrate that the observed parity-unfavored photoelectron emission is dominated by the angular momentum correlation between electron and ion, as shown in Fig. 4(e). In this process, the angular momentum transfer can be understood with a two-step model. First, the electron (angular momentum vector $\vec{J}_e$) absorbs the photon's angular momentum ($\vec{J}_\gamma$) solely, then transits from the $5p_0$ state to a d_0 state. Second, the electron and the excited ion ($\vec{J}_i$) do the precession about their total angular momentum vector $\vec{J} = \vec{J}_e + \vec{J}_i$, which is conservative after absorbing photons.

In the precession, the magnitude of $\vec{J}_e$ remains unchanged but its direction (i.e., the magnetic quantum number) will be changed drastically [13]. In fact, when the excited ion relaxes to the ground state, its angular momentum is correspondingly changed from $J_i = 1/2$ to $J_i = 3/2$. The transferred angular momentum along the quantum axis from the ion to the electron could be $\pm 2\hbar$ or $\pm 1\hbar$. Therefore, the electron state will be modified from d_0 to $d_{\pm 2}$ and $d_{\pm 1}$. Since the electron orbital $d_{\pm 2}$ has the minimum along the quantum axis and the maximum vertically, it causes the crosswise photoelectron emission.

This doubly excited dynamics can also be understood with the analogy of the autoionization of a two-electron excited state [38,39], if one views the residual five p electrons in the valence shell of the ion as an excited hole. As illustrated in Fig. 4(f), the angular momentum directions (i.e., orbital orientations) of the outmost excited electron and the hole are changed by their effective interaction during autoionization. In this angular momentum transfer, the electron thus can obtain the angular momentum component along the light polarization and correspondingly emits perpendicularly.

To justify the doubly excited dynamics, we have performed the experiment in circular polarization and successively varied the light intensity. In circularly polarized fields, the intermediate $5p$ state is not allowed to populate due to the confinement of the magnetic quantum number. Thus, the resonant pathway and the corresponding autoionization channel disappear. The mechanism will be dominated by the direct ionization pathway [see Fig. 4(b) for the measured intensity-resolved photoelectron energy spectrum and Fig. 4(d) for the corresponding schematic of direct pathway]. As a result, the photoelectron energy decreases linearly with increasing the light intensity, which is the evidence of the direct ionization pathway. Moreover, the photoelectron angular distribution [see Fig. 2(d)] and the relative photoelectron yield between the two ionic states [see green curve in Fig. 2(g)] return to normal.

Besides the parity-unfavored photoelectron emission, there is the rotation anomaly of the ATI lobes in small elliptically polarized fields, as seen in Fig. 2. In elliptically polarized fields, the parity-unfavored pathway and the direct ionization pathway will have comparable weights and their interference effect might be the reason for the abnormal electron rotation. Moreover, the influence of the asymmetric force driven by
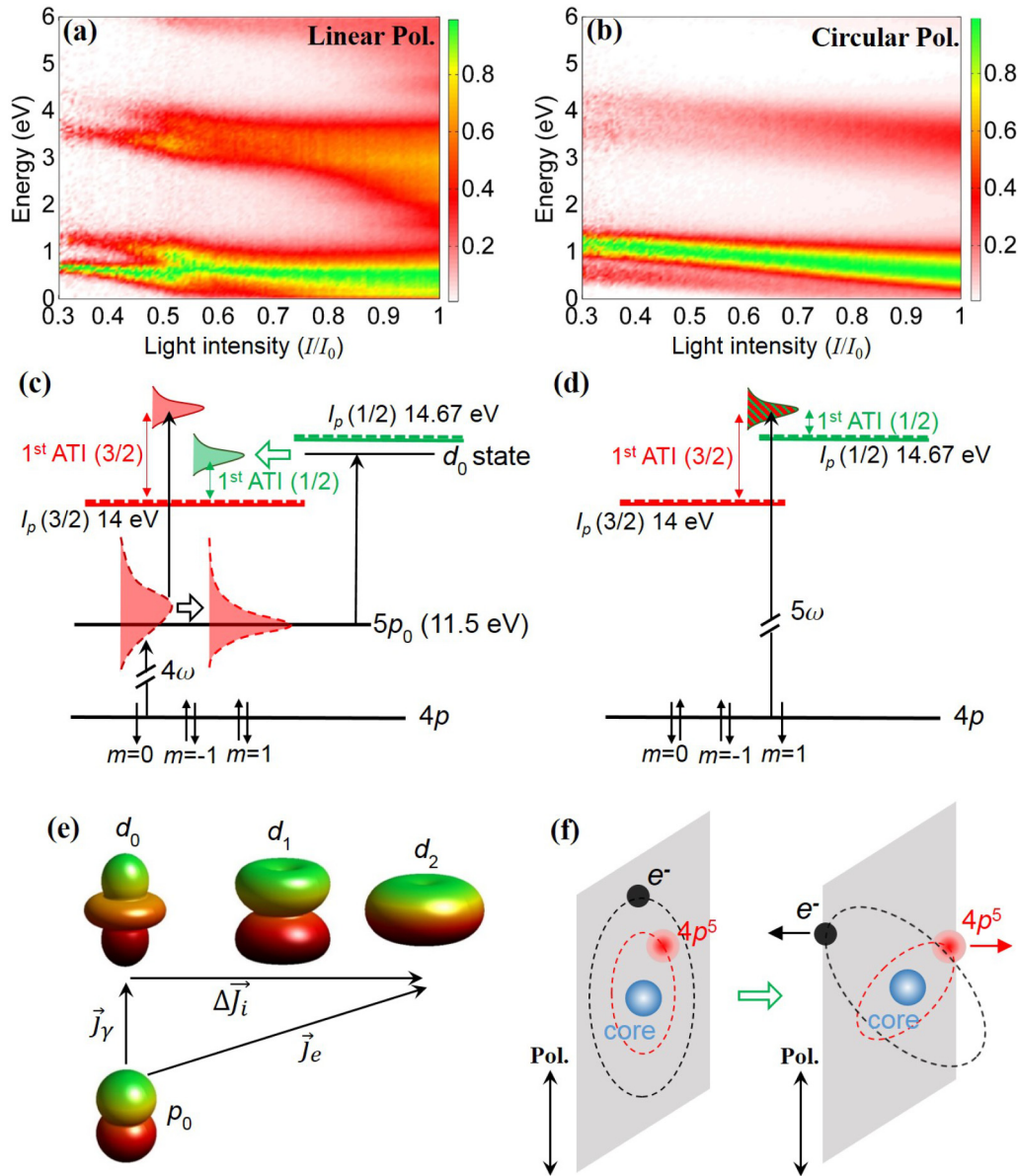
FIG. 4. (a),(b) Photoelectron energy spectra (angle-integrated) as a function of the light intensity in the linearly polarized field and the circularly polarized field, respectively. The maximum light intensity I_0 was calibrated at $\sim 8.0 \times 10^{13}$ W/cm^2. (c),(d) Ionization mechanism in the linearly polarized field and the circularly polarized field, respectively. In (c), the black hollow arrow represents the resonance process and the green hollow arrow represents the autoionization process. In the linearly polarized field, the presence of the resonant $5p$ state gives rise to the autoionization channel of the excited ionic state. In the circularly polarized field, both ionic states are ruled by the direct ionization pathway. (e) Change of the angular momentum vector of the outmost electron during the angular momentum transfer in the autoionization channel. $\vec{J}_\gamma$ is the spin angular momentum of photon, $\Delta \vec{J}_i$ is the variation of the angular momentum of the ion, and $\vec{J}_e$ is the electron angular momentum. (f) The alteration of the angular momentum directions [perpendicular to the orbit plane (dashed ellipse)] of the electron and the equivalent hole, caused by their repulsive interaction during the autoionization.

the elliptically polarized field on the electron correlation is also a non-negligible factor. More quantitative theoretical calculations are needed to explain this phenomenon.

In conclusion, we have studied the angular momentum transfer between the resonantly excited electron and the spin-orbit excited ion in multiphoton ionization. As a concrete performance of electron correlations, the ion is not the spectator in photoionization and it can share the angular momenta of photons with photoelectrons. Recent advances in attosecond science have allowed us to real-time trace and even control

the doubly excited electron dynamics, such as Fano resonance of photon-excited helium atoms [40–43]. The angular momentum transfer between the two excited particles in an atom or molecule would provide new insight into the fundamental many-body dynamics in photoionization and its temporal evolution would be an interesting topic coming within reach.

[1] C. B. Madsen, F. Anis, L. B. Madsen, and B. D. Esry, Phys. Rev. Lett. **109**, 163003 (2012).

[2] R. E. F. Silva, F. Catoire, P. Rivière, H. Bachau, and F. Martín, Phys. Rev. Lett. **110**, 113001 (2013).

[3] J. Wu, M. Kunitski, M. Pitzer, F. Trinter, L. Ph. H. Schmidt, T. Jahnke, M. Magrakvelidze, C. B. Madsen, L. B. Madsen, U. Thumm, and R. Dörner, Phys. Rev. Lett. **111**, 023002 (2013).

[4] X. Sun, M. Li, Y. Shao, M.-M. Liu, X. Xie, Y. Deng, C. Wu, Q. Gong, and Y. Liu, Phys. Rev. A **94**, 013425 (2016).

[5] S. Chelkowski, A. D. Bandrauk, and P. B. Corkum, Phys. Rev. Lett. **113**, 263005 (2014).

[6] C. T. L. Smeenk, L. Arissian, B. Zhou, A. Mysyrowicz, D. M. Villeneuve, A. Staudte, and P. B. Corkum, Phys. Rev. Lett. **106**, 193002 (2011).

[7] A. Hartung, S. Eckart, S. Brennecke, J. Rist, D. Trabert, K. Fehre, M. Richter, H. Sann, S. Zeller, K. Henrichs, G. Kastirke, J. Hoehl, A. Kalinin, M. S. Schöffler, T. Jahnke, L. Ph. H. Schmidt, M. Lein, M. Kunitski, and R. Dörner, Nat. Phys. **15**, 1222 (2019).

[8] T. Otobe, K. Yabana, and J. I. Iwata, Phys. Rev. A **69**, 053404 (2004).

[9] U. Fano and D. Dill, Phys. Rev. A **6**, 185 (1972).

[10] D. Dill, Phys. Rev. A **6**, 160 (1972).

[11] U. Fano and D. Dill, Phys. Rev. Lett. **29**, 1203 (1972).

[12] D. Dill, Phys. Rev. A **7**, 1976 (1973).

[13] D. Dill, A. F. Starace, and S. T. Manson, Phys. Rev. A **11**, 1596 (1975).

[14] A. F. Starace, S. T. Manson, and D. J. Kennedy, Phys. Rev. A **9**, 2453 (1974).

[15] I. Barth and O. Smirnova, Phys. Rev. A **88**, 013401 (2013).

[16] A. Hartung *et al.*, Nat. Photon. **10**, 526 (2016).

[17] M.-M. Liu, Y. Shao, M. Han, P. Ge, Y. Deng, C. Wu, Q. Gong, and Y. Liu, Phys. Rev. Lett. **120**, 043201 (2018).

[18] D. Trabert, A. Hartung, S. Eckart, F. Trinter, A. Kalinin, M. Schöffler, L. Ph. H. Schmidt, T. Jahnke, M. Kunitski, and R. Dörner, Phys. Rev. Lett. **120**, 043202 (2018).

[19] M. Han, P. Ge, M.-M. Liu, Q. Gong, and Y. Liu, Phys. Rev. A **99**, 023404 (2019).

[20] E. Goulielmakis *et al.*, Nature (London) **466**, 739 (2010).

[21] H. J. Wörner and P. B. Corkum, J. Phys. B **44**, 041001 (2011).

[22] A. Fleischer, H. J. Wörner, L. Arissian, L. R. Liu, M. Meckel, A. Rippert, R. Dörner, D. M. Villeneuve, P. B. Corkum, and A. Staudte, Phys. Rev. Lett. **107**, 113003 (2011).

[23] L. Fechner, N. Camus, J. Ullrich, T. Pfeifer, and R. Moshammer, Phys. Rev. Lett. **112**, 213001 (2014).

[24] I. Jordan, M. Huppert, S. Pabst, A. S. Kheifets, D. Baykusheva, and H. J. Wörner, Phys. Rev. A **95**, 013404 (2017).

[25] Y. Shao, M. Li, M.-M. Liu, X. Sun, X. Xie, P. Wang, Y. Deng, C. Wu, Q. Gong, and Y. Liu, Phys. Rev. A **92**, 013415 (2015).

[26] R. Dörner, V. Mergel, O. Jagutzki, L. Spielberger, J. Ullrich, R. Moshammer, and H. Schmidt-Böcking, Phys. Rep. **330**, 95 (2000).

[27] J. Ullrich, R. Moshammer, A. Dorn, R. Dorner, L. Ph. H. Schmidt, and H. Schmidt Bocking, Rep. Prog. Phys. **66**, 1463 (2003).

[28] M. Bashkansky, P. H. Bucksbaum, and D. W. Schumacher, Phys. Rev. Lett. **60**, 2458 (1988).

[29] S. P. Goreslavski, G. G. Paulus, S. V. Popruzhenko, and N. I. Shvetsov-Shilovski, Phys. Rev. Lett. **93**, 233002 (2004).

[30] M. Li, Y. Liu, H. Liu, Q. Ning, L. Fu, J. Liu, Y. Deng, C. Wu, L.-Y. Peng, and Q. Gong, Phys. Rev. Lett. **111**, 023006 (2013).

[31] L.-Y. Peng and Q. Gong, Comput. Phys. Commun. **181**, 2098 (2010).

[32] V. Mosert and D. Bauer, Comput. Phys. Commun. **207**, 452 (2016).

[33] A. Muhlpfordt and U. Even, J. Chem. Phys. **103**, 4427 (1995).

[34] V. L. Sukhorukov, I. D. Petrov, M. Schafer, F. Merkt, M.-W. Ruf, and H. Hotop, J. Phys. B **45**, 092001 (2012).

[35] L. Fechner, N. Camus, A. Krupp, J. Ullrich, T. Pfeifer, and R. Moshammer, Phys. Rev. A **92**, 051403(R) (2015).

[36] M. Nakano, T. Otobe, and R. Itakura, Phys. Rev. A **95**, 063404 (2017).

[37] A. P. Fidler, H. J. B. Marroux, E. R. Warrick, E. Bloch, W. Cao, S. R. Leone, and D. M. Neumark, J. Chem. Phys. **151**, 114305 (2019).

[38] U. Fano and C. H. Greene, Phys. Rev. A **22**, 1760 (1980).

[39] C. H. Greene, Phys. Rev. Lett. **44**, 869 (1980).

[40] C. Ott, A. Kaldun, P. Raith, K. Meyer, M. Laux, J. Evers, C. H. Keitel, C. H. Greene, and T. Pfeifer, Science **340**, 716 (2013).

[41] C. Ott *et al.*, Nature (London) **516**, 374 (2014).

[42] A. Kaldun, A. Blättermann, V. Stooß, S. Donsa, H. Wei, R. Pazourek, S. Nagele, C. Ott, C. D. Lin, J. Burgdörfer, and T. Pfeifer, Science **354**, 738 (2016).

[43] C. Ott, L. Aufleger, T. Ding, M. Rebholz, A. Magunia, M. Hartmann, V. Stooss, D. Wachs, P. Birk, G. D. Borisova, K. Meyer, P. Rupprecht, C. daCostaCastanheira, R. Moshammer, A. R. Attar, T. Gaumnitz, Z. H. Loh, S. Dusterer, R. Treusch, J. Ullrich *et al.*, Phys. Rev. Lett. **123**, 163201 (2019).